Journal of the Taiwan Institute of Chemical Engineers 80 (2017) 695–700

Contents lists available at ScienceDirect

Journal of the Taiwan Institute of Chemical Engineers

journal homepage: www.elsevier.com/locate/jtice

Improved efficiency of perovskite photovoltaics based on Ca-doped methylammonium lead halide

Ming-Chung Wu[a,b,c,*], Tzu-Hao Lin[a], Shun-Hsiang Chan[a], Wei-Fang Su[d]

[a] Department of Chemical and Materials Engineering, Chang Gung University, Taoyuan 33302, Taiwan
[b] Center for Reliability Sciences & Technologies, Chang Gung University, Taoyuan 33302, Taiwan
[c] Division of Neonatology, Department of Pediatrics, Chang Gung Memorial Hospital, Taoyuan 33305, Taiwan
[d] Department of Materials Science and Engineering, National Taiwan University, Taipei 10617, Taiwan

ARTICLE INFO

Article history:
Received 4 May 2017
Revised 2 September 2017
Accepted 4 September 2017
Available online 21 September 2017

Keywords:
Methylammonium lead halide
Morphology
Calcium
Perovskite solar cell

ABSTRACT

Hybrid lead halide perovskite structured materials have created enormous expectations for low-cost and high-performance optoelectronic devices. The light-harvesting active layer of perovskite solar cell consists of hybrid organic-inorganic lead halide-based material. In this study, we successfully fabricated the perovskite photovoltaics with partial substitution of the lead cation (Pb^{2+}) with calcium ion (Ca^{2+}). The incorporation of Ca^{2+} into the original structure was analyzed to observe the doping effect on the crystalline structure and the optical properties. Moreover, UV–vis spectra showed the decreased bandgap with ascending the dopants Ca^{2+} amount. 1.0 mol% Ca-doped perovskite film has the lower emission energy, and it shows the low recombination behavior. After optimizing the perovskite solar cells, the V_{oc} is increased from 0.93 to 0.98 V, the J_{sc} is increased from 17.4 to 19.1 mA/cm^2 and the power conversion efficiency is enhanced from 10.7 to 12.9% by using 1.0 mol% Ca-doped perovskite material.

1. Introduction

Hybrid lead halide photovoltaic device has been considered as one of the promising technologies for future photovoltaics, because of the rapid rise of the achievable power conversion efficiency (PCE) [1]. Currently, the certified PCE approached to 22.1% since the initial report of 3.8% demonstrated by Miyasaka group in 2009 [2–10]. The structure of perovskite materials are similar to the mineral calcium titanium oxide, and the chemical formula is ABX_3, where A, B, and X are denoted as organic cation, metal ion, and halide, respectively [11,12]. Most of the perovskite materials used as emerging photovoltaic devices contain the lead component. The existence of lead can cause toxicological and environmental issues [13–15]. Therefore, many research groups focused on discovering the new perovskite materials that can replace the lead and improve photovoltaic performance. In addition, the hybrid perovskite materials exhibit high absorption characteristics, tunable bandgap, long diffusion length, and high carrier mobility [16–23].

Recently, the lead-free perovskite solar materials based on Sn^{2+} have been studied. However, the PCE of tin-based perovskite solar cells is not over 7% due to the unstable properties and poor film coverage [24–26]. Moreover, controlling the Sn–Pb ratio can tune the absorption of Sn–Pb binary metal perovskites. Up to now, the binary metal-based perovskite solar cells have achieved over PCE of 13% [24,27–29]. It is necessary to seek the replacements or substitutions for achieving high performance lead-free or lead-reduced perovskite solar cells. Moreover, partial substitution of the Pb^{2+} by doping Al^{3+} was able to obtain the high quality perovskite film and therefore increase the PCE [30]. High quality In-Pb perovskite film was studied, and it showed the multiple ordered crystal orientations. The efficient charge transport occurred at multiple directions so that it can improve photovoltaic performance [31]. The perovskite thin film with small amounts of Sr^{2+} doping ($0.01 \leq Sr/Pb \leq 0.05$) can enhance the charge carrier lifetime and decrease surface roughness [32]. Importantly, the metal ion can slightly change the crystallinity, optoelectronic characteristics, or optical properties of the perovskite absorber layer. Therefore, some of the research groups are focusing on the partial substitution of Pb^{2+} to fabricate the perovskite solar cells. The Pb^{2+} position of hybrid perovskite materials with slightly replaced by Cd^{2+} or Ca^{2+} showed the red shift of the absorption spectra. The toxicity of Cd^{2+} limited its practical application. Ca-doped perovskite material exhibited low emission values from the cathodoluminescence spectra, so it could display low recombination behavior [33]. In addition, Pazoki et al. showed three alkaline-earth metals (Ca, Sr, and

* Corresponding author at: Department of Chemical and Materials Engineering, Chang Gung University, Taoyuan 33302, Taiwan.
E-mail addresses: mingchungwu@mail.cgu.edu.tw, mingchungwu@ntu.edu.tw (M.-C. Wu).

http://dx.doi.org/10.1016/j.jtice.2017.09.004
1876-1070/

Ba) are the potential candidates for replacing the lead to fabricating the perovskite materials due to the Ca^{2+}, Sr^{2+}, and Ba^{2+} have similar size and same charge as Pb^{2+} [36].

In this study, we successfully fabricated the perovskite photovoltaics with partial substitution of Pb^{2+} by doping Ca^{2+}. The incorporation effect of Ca^{2+} was analyzed to observe the changes in crystalline structure and optoelectronic properties. X-ray diffraction (XRD) results showed the increased (110) facet with increasing the Ca^{2+} concentration in methylammonium lead halide. Moreover, UV–vis spectra showed the decreased band gap with ascending the Ca^{2+} doping concentration. The results indicated that it could enhance the utilization of visible light. After optimizing the perovskite photovoltaics, the open circuit voltage (V_{oc}) and the short-circuit current density (J_{sc}) are increased and the PCE is also enhanced by using 1.0 mol% Ca-doped perovskite material.

2. Experimental details

2.1. Materials preparation

The synthesis of methylammonium iodide (MAI) was delivered according to the literature [34]. The precursor solution was prepared by mixing lead chloride ($PbCl_2$, 99.999%, Aldrich) and with MAI a molar ratio of 1.0: 2.6 in anhydrous dimethylformamide (DMF) ($HCON(CH_3)_2$, 99.8%, Aldrich) which is about 40.0 wt.%. For the preparation of Ca-doped perovskite solution, MAI, $PbCl_2$, and calcium iodide (CaI_2, 99%, Aldrich) were dissolved in DMF with the desired molar ratio.

TiO_2 precursor solution was prepared by the following steps. At first, 375 μL of titanium isopropoxide ($Ti(OCH(CH_3)_2)_4$, 98% + , Acros) was added to 2.5 mL of ethanol (99.5%, Shimakyu's Pure. Chemicals) to obtain the solution A. After that, 35 μL of 2.0 M HCl solution was dropped into 2.5 mL of ethanol to obtain the solution B. Finally, solution A was mixed with solution B with the volume ratio of 1.0, and the mixed solution were placed in ice bath with the continuous stirring. Finally, we obtained the TiO_2 precursor solution to prepare the hole blocking layer.

For the preparation of spiro-OMeTAD ($C_{81}H_{68}N_4O_8$, 99%, STAREK Scientific Co., Ltd) electron blocking layer, 520 mg of lithium-bis-(trifluoromethanesulfonyl)imide, Li-TFSI, ($CF_3SO_2NLiSO_2CF_3$, 99.95%, Aldrich) was dissolved in 1.0 mL acetonitrile (CH_3CN, 99.5%, Acros) at first. Then, 80 mg spiro-OMeTAD, 28.5 μL 4–tert–butylpyridine (tBP) ($C_9H_{13}N$, 96%, Aldrich), and 17.5 μL Li-TFSI solution in 1.0 mL chlorobenzene (C_6H_5Cl, 99.8%, Acros) were mixed together with continuous stirring to obtain the spiro-OMeTAD solution. Finally, the spiro-OMeTAD solution was used to coat the electron blocking layer.

2.2. Fabrication of the perovskite photovoltaic devices

The photovoltaic devices in this study were fabricated by cleaned fluorine-doped tin oxide (FTO) glass substrates (7Ω, STAREK Scientific Co., Ltd) as the transparent electrodes. We cleaned the FTO glass substrates sequentially by ultrasonic vibration using detergent for 5 min, alkalis liquid (DI water: hydrogen peroxide: ammonia solution = 5.0:1.0:1.0) for 40 min, methanol for 20 min, and isopropanol for 20 min. Finally, the FTO glass substrates were exposed by an ultraviolet ozone cleaner (FrontMaterials Co., Ltd).

TiO_2 precursor solution was spin-coated on the FTO glass substrates at 1000 rpm for 40 s, and it was subsequently calcined at 550 °C for 30 min to form the TiO_2 compact layer as the hole blocking layer of the perovskite solar cells. After that, the various Ca^{2+} doped perovskite solution was spin-coated and annealed on the hot plate at 100 °C for 1 h in a constant relative humidity glovebox (humidity maintain about 1.0% RH). Then, spiro-OMeTAD solution was spin-coated at 4000 rpm for 30 s in a constant relative humidity chamber. Finally, the gold electrodes with a 100 nm thickness were thermally evaporated on the surface of spiro-OMeTAD compact layer by using a shadow mask with 0.09 cm^2 area.

Table 1
List of the bandgap of various Ca-doped perovskite film with different Ca doping levels.

Material	Ca/Ca + Pb (%)	Bandgap (eV)
$CH_3NH_3PbI_{3-x}Cl_x$	0.0	1.569
$CH_3NH_3Pb_{0.99}Ca_{0.01}I_{3-x}Cl_x$	1.0	1.568
$CH_3NH_3Pb_{0.98}Ca_{0.02}I_{3-x}Cl_x$	2.0	1.566
$CH_3NH_3Pb_{0.95}Ca_{0.05}I_{3-x}Cl_x$	5.0	1.562
$CH_3NH_3Pb_{0.90}Ca_{0.10}I_{3-x}Cl_x$	10.0	1.542

2.3. Characterization

The crystal structure was analyzed by X-ray diffractometer (D2 phaser, Bruker) with CuKα radiation. The scanning electron microscope (SNE-4500 M, SEC) was used to observe the surface microstructure of various Ca-doped perovskite films. The atomic force microscope (Bruner Multimode2-U-NSV, Bruker) in tapping mode was used to characterize the surface topography and root-mean-square roughness of various Ca-doped perovskite films. The spectra of Kubelka–Munk function of the various perovskite films were measured by a UV–vis spectrometer (V-650, Jasco) equipped with the 60 mm integrating spheres. The current-voltage characteristics of perovskite solar cells were measured by the source meter (Keithley 2410) under a simulated Air-Mass 1.5 sunlight at 100 mW/cm^2 (Newport-69,920 solar simulator). The steady-state photoluminescence (PL) was carried out under the excitation of a 440 nm continuous-wave laser (PDLH-440-25, DongWoo Optron Co. Ltd.). The PL signals were analyzed by a detector system (PDS-1, DongWoo Optron Co. Ltd.) and standard photon-counting electronics using a monochromator (Monora 150i, DongWoo Optron Co. Ltd.). TRPL spectroscopy was performed using the time-resolved single-photon-counting set-up (WELLS-001 FX, DongWoo Optron Co. Ltd.). The external quantum efficiency (EQE) of perovskite photovoltaic devices were measured using a monochromatic incident photon-to-electron conversion efficiency spectrometer (EQE-R-3011, Enli Technology Co. Ltd), with the monochromatic light wavelength ranging from 300 to 850 nm. X-ray photoelectron spectrometry (XPS, VG ESCA Scientific, Theta Probe) was used to measure Ca doping concentration of various perovskite film by using Al Kα radiation (1486.6 eV) with a photoelectron 53° take off angle under high vacuum ($\sim 10^{-10}$ torr).

3. Results and discussion

XRD patterns of various Ca-doped perovskite ($CH_3NH_3Pb_{1-y}Ca_yI_{3-x}Cl_x$) film with different Ca doping levels are shown in Fig. 1(a), where y is 0.00, 0.01, 0.02, 0.05 and 0.10, respectively. For the (001) facet of PbI_2, the intensity of PbI_2 decreased with increasing the Ca doping level. In Fig. 1(b), increasing the Ca doping level led to a slight shift of (110) facet to the small diffraction angle. The results showed that the structure was affected by the change of metal cation in the perovskite structure.

Fig. 2 shows the Kubelka–Munk function spectra of various Ca-doped perovskite film with different Ca doping levels. The Kubelka–Munk equation was used to calculate the optical absorption coefficient (K/S) [35]. Fig. 2(a) shows that the presence of Ca^{2+}leads to red-shift of the absorption spectrum. Notably, the bandgap decreased from 1.569 to 1.542 eV with increasing Ca^{2+} concentration as shown in Fig. 2(b) and Table 1.

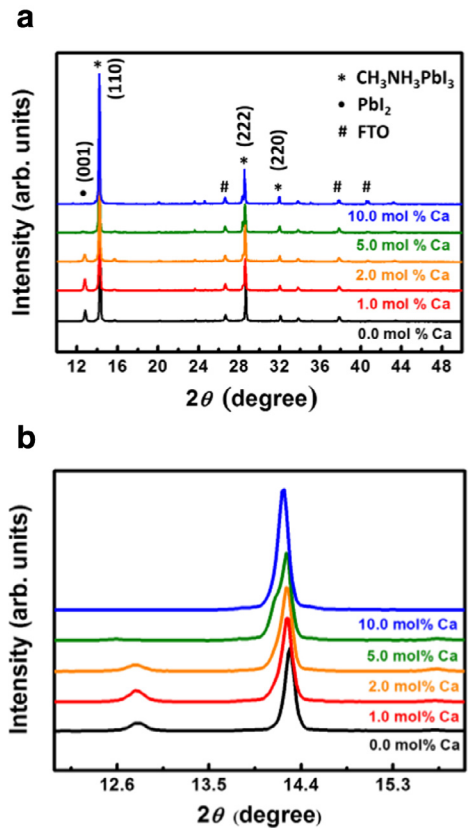

Fig. 1. (a) XRD patterns of various perovskite filmswith different Ca doping levels. (b) Magnified patterns of plane (110) diffraction peaks of various perovskite film with different Ca doping levels.

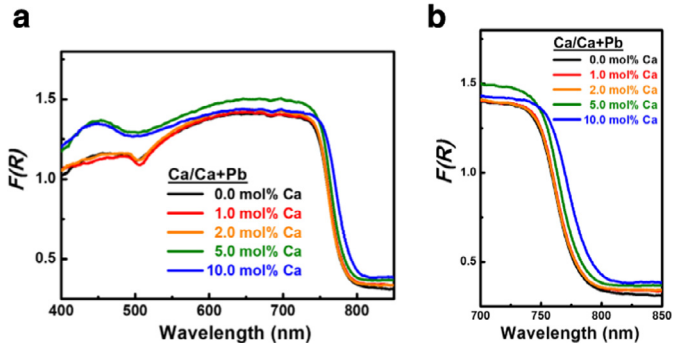

Fig. 2. (a) Diffuse reflectace spectra converted by Kubelka–Munk function of various perovskite film with the different Ca doping levels. (b) Magnified spectra between the wavelength ranged from 700 to 850 nm.

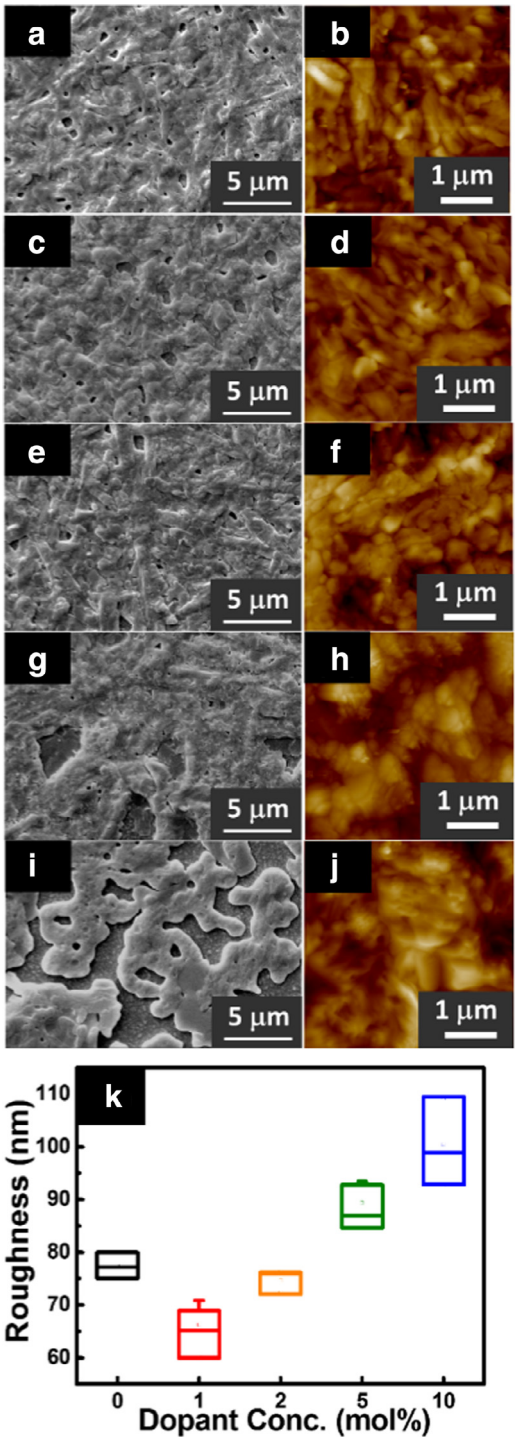

Fig. 3. SEM images and AFM topographical images of various perovskite filmswith different Ca doping levels, including (a,b) non-doped, (c,d) 1.0 mol%, (e,f) 2.0 mol%, (g,h) 5.0 mol%, and (i,j) 10.0 mol%. (k) The root-mean-square roughness of various Ca-doped perovskite films analyzed by AFM.

In order to examine the topography of the various Ca-doped perovskite film, SEM and AFM were applied to analyze. Fig. 3 is the SEM images of perovskite with various Ca doping levels. In Fig. 3(a), we can observe that there existed some pinholes on the film, which would be hampered for the electron and hole transport. When Ca doping level achieved to 1.0 mol%, a number of pinholes decreased (Fig. 3(c)). However, the pinholes occurred apparently, when Ca doping level was higher than 1.0 mol% (Fig. 3(e), (g), and (i)). The roughness of the various Ca-doped perovskite films was measured by AFM (Fig. 3(k)). The Ca-doped perovskite film with 1.0 mol% doping level exhibited the smallest root-mean-square roughness among all Ca-doped perovskite films.

The architecture of our n-i-p planar structure is FTO/TiO_2 compact layer/Ca-doped perovskite active layer/spiro-OMeTAD/Au electrode as shown in Fig. 4(a). The J-V curves were used to observe the Ca doping effects as shown in Fig. 4(b), and the plots of photovoltaic performances of perovskite photovoltaic devices with various Ca doping levels are shown in Fig. 4(c)–(f). The characteristics of photovoltaic devices with various Ca doping levels are summarized in Table 2. The $CH_3NH_3PbI_{3-x}Cl_x$ standard sample of perovskite solar cell showed the average power conversion efficiency of 10.7%, V_{oc} of 0.93 V, J_{SC} of 17.4 mA/cm^2, and fill

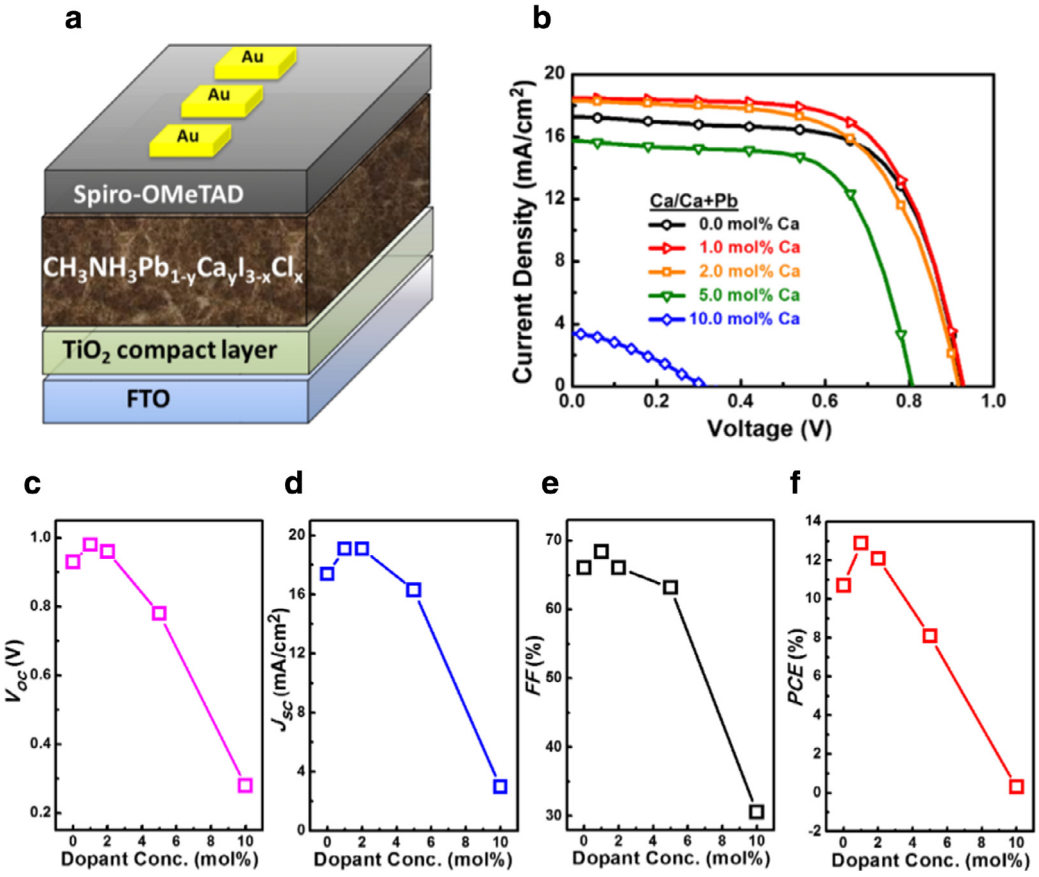

Fig. 4. (a) The schematic diagram of perovskite solar cell structure. (b) J-V curves and (c) the plots of photovoltaic characteristics of various perovskite solar cells with different Ca doping levels.

Table 2
Characteristics of perovskite solar cells with different Ca doping levels.

Ca/Ca + Pb (%)	V_{oc} (V)	J_{sc} (mA/cm^2)	*FF* (%)	*PCE* (%)
0.0	0.93 ± 0.02	17.4 ± 0.1	66.1 ± 1.4	10.7 ± 0.1
1.0	0.98 ± 0.02	19.1 ± 0.4	68.4 ± 1.6	12.9 ± 0.6
2.0	0.96 ± 0.02	19.1 ± 0.4	66.1 ± 0.8	12.1 ± 0.2
5.0	0.78 ± 0.04	16.3 ± 1.2	63.2 ± 2.9	8.0 ± 0.4
10.0	0.32 ± 0.11	3.0 ± 0.5	30.6 ± 4.9	0.3 ± 0.1

Table 3
Summary of measured fast decay time (τ_1), intermediate decay time (τ_2), slow decay time (τ_3), and PL average decay (τ_{avg}) for $CH_3NH_3Pb_{1-y}Ca_yI_{3-x}Cl_x$/ TiO_2 compact layer/ FTO.

Ca/Ca + Pb (%)	A_1 (10^{-3})	τ_1 (ns)	A_2 (10^{-3})	τ_2 (ns)	A_3 (10^{-2})	τ_3 (ns)	τ_{avg} (ns)
0.0	3.1	4080	1.8	175	1.7	7.8	12.6
1.0	0.7	1325	2.4	118	1.5	3.1	4.5
2.0	5.1	1311	0.2	138.6	3.8	4.7	14.8
5.0	6.4	788	0.4	131	5.3	8.5	32.8
10.0	0.1	901	0.2	121	3.2	4.5	37.3

factor (FF) of 66.1%. When the perovskite doping level reached to 1.0 mol%, the Ca-doped perovskite photovoltaic device exhibited a slight improvement in all the performance parameters, which are average PCE of 12.9% with V_{oc} of 0.98 V, J_{sc} of 19.1 mA/cm^2, and FF of 68.4%. Over 20 photovoltaic devices were fabricated and tested for each parameter in this study. However, when doping level was higher than 1.0 mol%, all the photovoltaic characteristics were getting worse, and these results are consistent with the SEM images and AFM topographical images.

We studied the charge carrier dynamics of the various Ca-doped perovskite films by photoluminescence (PL) spectroscopy and time-resolved photoluminescence (TRPL) technique (Fig. 5). From the photoluminescence spectra (Fig. 5(a)), 1.0 mol% Ca-doped perovskite films presented weaker PL signal, because of the PL quenching effect. Therefore, 1.0 mol% Ca-doped perovskite film had the lower emission energy, and it displayed the weaker recombination behavior. To further confirm the charge carrier dynamics, we tested these samples by TRPL as shown in Fig. 5(b). The TRPL spectra were fitted by the triexponential equation and the average lifetime (τ_{avg}) was listed in Table 3. The τ_{avg} of non-doped perovskite film is 12.6 ns. For Ca-doped perovskite films, the τ_{avg} are 4.5 ns for 1.0 mol% dopant, 14.8 ns for 2.0 mol% dopant, 32.8 ns for 5.0 mol% dopant, and 37.3 ns for 10.0 mol% dopant. From the TRPL results, 1.0 mol% Ca-doped perovskite film exhibited the shortest lifetime (τ_{avg}~4.5 ns), so the lowest recombination rate could occur in this sample. The 1.0 mol% Ca-doped perovskite solar cell displayed higher EQE comparing with non-doped perovskite solar cell (Fig. 6). The full spectral range was increased for 1.0 mol% Ca-doped perovskite solar cell with increasing absorption behavior due to the lower bandgap than the non-doped perovskite solar cells. In addition, 1.0 mol% Ca-doped perovskite solar cell shows higher crystallinity (Fig. 1), so it can excite more electrons. The J_{sc} of 1.0 mol% Ca-doped perovskite solar cell (19.1 mA/cm^2) is higher than the non-doped perovskite solar cell (17.4 mA/cm^2) by integrating the overlap of the EQE spectra with the AM1.5 G solar photon flux in the range of 300 nm to 750 nm.

Finally, we compared the stability of the non-doped and 1.0 mol% Ca-doped perovskite solar cell measurement in the condition of 25 °C and 50%RH. The two perovskite solar cells are not encap-

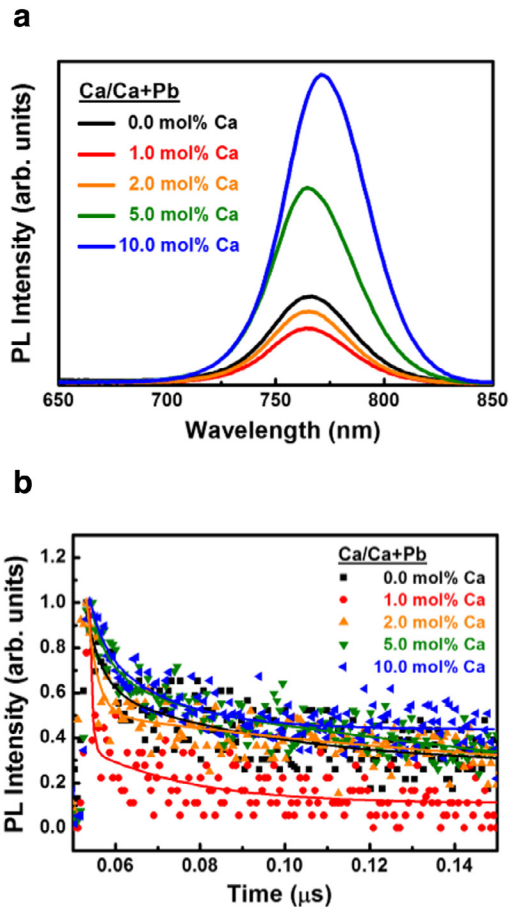

Fig. 5. (a) Photoluminescence spectra and (b) the time-resolved photoluminescence decay transients of various perovskite films with different Ca doping levels.

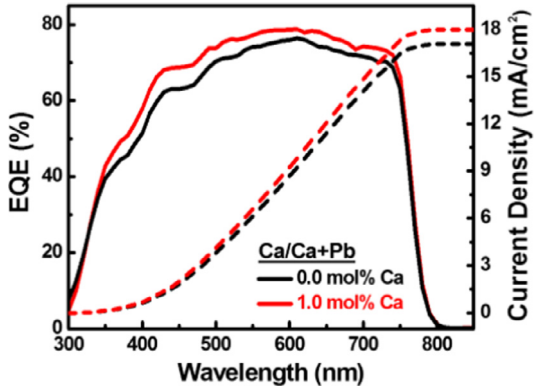

Fig. 6. EQE spectra of non-doped perovskite solar cell and 1.0 mol% Ca-doped perovskite solar cell.

sulated, and stored separately in the two kinds of glove box system, which one is humidity maintain about 1.0% relative humidity, and the other is oxygen and humidity maintain < 0.1 ppm. In the glovebox system with 1.0%RH, the 1.0 mol% Ca-doped perovskite solar cell become more stable than the non-doped perovskite solar cell. After 744 h (31 days), the 1.0 mol% Ca-doped perovskite solar cell reached ~79% of the normalized PCE (Fig. 7(a)). In the glovebox system with oxygen and humidity maintain < 0.1 ppm, the 1.0 mol% Ca-doped perovskite solar cell still exhibits high stability. 1.0 mol% Ca-doped perovskite solar cell reached ~91% of the normalized PCE after 744 h (Fig. 7(b)). The enhanced stability is attributed to the stable Ca ion oxidation states in 1.0 mol% Ca-doped perovskite film. Moreover, the chemical compositions of various perovskite active layer were measured by XPS to obtain the atomic ratios of Ca/Ca + Pb. For XPS spectra of Pb 4f, the two peak positions at 141.8 eV and 137.9 eV are corresponding to Pb $4f_{5/2}$ and Pb $4f_{7/2}$ [37, 38]. The peak position of Ca $2p_{3/2}$ is 346.6 eV [39]. After analyzing the XPS data, the atomic ratios of Ca/Ca + Pb for various perovskite active layer are shown in Table 4.

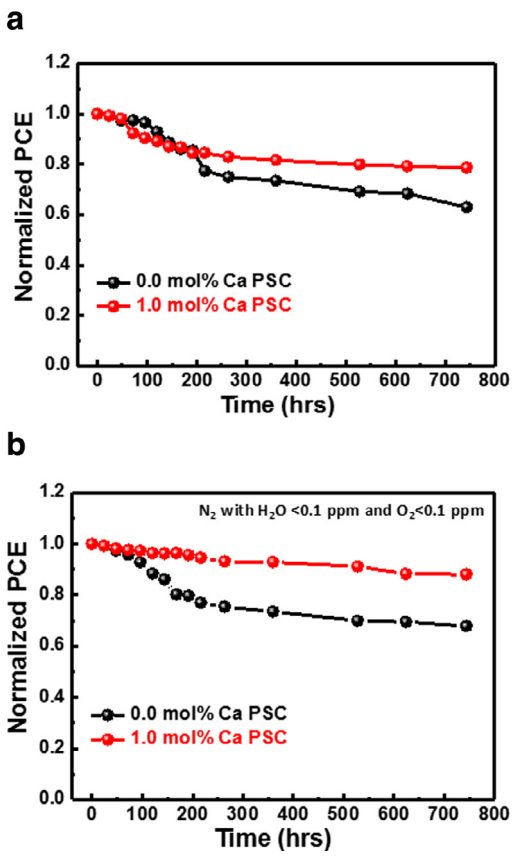

Fig. 7. Normalized PCE of PCSs with the non-doped and 1.0 mol% Ca-doped perovskite solar cell,which are stored in two conditions, (a)1.0% RH and (b) oxygen and humidity maintain < 0.1 ppm. (For interpretation of the references to color in this figure legend, the reader is referred to the web version of this article.)

Table 4
Theoretical and experimental atomic ratios of Ca/Ca + Pb in non-doped and various Ca-doped perovskite active layer.

Sample name	Ca/Ca + Pb(%)	
	Theoetical value	XPS analysis
$CH_3NH_3PbI_{3-x}Cl_x$	0.0	0.0
$CH_3NH_3Pb_{0.99}Ca_{0.01}I_{3-x}Cl_x$	1.0	1.4
$CH_3NH_3Pb_{0.98}Ca_{0.02}I_{3-x}Cl_x$	2.0	2.8
$CH_3NH_3Pb_{0.95}Ca_{0.05}I_{3-x}Cl_x$	5.0	6.4
$CH_3NH_3Pb_{0.90}Ca_{0.10}I_{3-x}Cl_x$	10.0	11.0

4. Conclusion

We successfully fabricated the n-i-p type planar structure of Ca-doped perovskite photovoltaic devices and enhanced the PCE by doping Ca^{2+} into the perovskite structured materials. The Ca dopant can reduce the bandgap and extend the absorption to the visible range. After optimizing Ca-doped perovskite solar cells, the V_{oc} is increased from 0.93 to 0.98 V, the J_{sc} is enhanced from 17.4 to 19.1 mA/cm^2, and the PCE can be improved from 10.7 to 12.9% by using 1.0 mol% Ca-doped perovskite active layer.

Acknowledgments

The authors appreciate Chair Prof. Yang-Fang Chen at National Taiwan University, Dr. Ming-Tao Lee at National Synchrotron Radiation Research Center (BL-13A1), and Dr. Tz-Feng Lin at Chang Gung University for useful discussion and suggestions. The authors acknowledge the financial support from Ministry of Science and Technology, Taiwan (MOST 106-2221-E-182-057-MY3, MOST 106-2119-M-002-030 and MOST 106-2632-E-182-001) and Chang Gung Memorial Hospital, Linkou (CMRPD2F0161 and BMRPC74).

References

[1] Zhao Y, Liu J, Lu X, Gao Y, You X, Xu X. Improving the efficiency of perovskite solar cells through optimization of the $CH_3NH_3PbI_3$ film growth in solution process method. App Surf Sci 2015;359:560–6.
[2] Bi D, Tress W, Dar MI, Gao P, Luo J, Renevier C, et al. Efficient luminescent solar cells based on tailored mixed-cation perovskites. Sci Adv 2016;2:1501170.
[3] Saliba M, Matsui T, Domanski K, Seo J-Y, Ummadisingu A, Zakeeruddin SM, et al. Incorporation of rubidium cations into perovskite solar cells improves photovoltaic performance. Science 2016;354:206–9.
[4] Saliba M, Matsui T, Seo J-Y, Domanski K, Correa-Baena J-P, Nazeeruddin MK, et al. Cesium-containing triple cation perovskite solar cells: improved stability, reproducibility and high efficiency. Energy Environ Sci 2016;9:1989–97.
[5] Saliba M, Orlandi S, Matsui T, Aghazada S, Cavazzini M, Correa-Baena J-P, et al. A molecularly engineered hole-transporting material for efficient perovskite solar cells. Nat Energy 2016;1:15017.
[6] Yang WS, Noh JH, Jeon NJ, Kim YC, Ryu S, Seo J, et al. High-performance photovoltaic perovskite layers fabricated through intramolecular exchange. Science 2015;348:1234–7.
[7] Kojima A, Teshima K, Shirai Y, Miyasaka T. Organometal halide perovskites as visible-light sensitizers for photovoltaic cells. J Am Chem Soc 2009;131:6050–1.
[8] Della Gaspera E, Peng Y, Hou Q, Spiccia L, Bach U, Jasieniak JJ, et al. Ultra-thin high efficiency semitransparent perovskite solar cells. Nano Energy 2015;13:249–57.
[9] Huang F, Dkhissi Y, Huang W, Xiao M, Benesperi I, Rubanov S, et al. Gas-assisted preparation of lead iodide perovskite films consisting of a monolayer of single crystalline grains for high efficiency planar solar cells. Nano Energy 2014;10:10–18.
[10] Xiao M, Huang F, Huang W, Dkhissi Y, Zhu Y, Etheridge J, et al. A fast deposition-crystallization procedure for highly efficient lead iodide perovskite thin–film solar cells. Angew Chem Int Edit 2014;126:1–7.
[11] Gao P, Grätzel M, Nazeeruddin MK. Organohalide lead perovskites for photovoltaic applications. Energy Environ Sci 2014;7:2448–63.
[12] Peña MA, Fierro JLG. Chemical structures and performance of perovskite oxides. Chem Rev 2001;101:1981–2018.
[13] Babayigit A, Duy Thanh D, Ethirajan A, Manca J, Muller M, Boyen H-G, et al. Assessing the toxicity of Pb- and Sn-based perovskite solar cells in model organism Danio rerio. Sci Rep 2016;6:18721.
[14] Babayigit A, Ethirajan A, Muller M, Conings B. Toxicity of organometal halide perovskite solar cells. Nat Mater 2016;15:247–51.
[15] Benmessaoud IR, Mahul-Mellier A-L, Horvath E, Maco B, Spina M, Lashuel HA, et al. Health hazards of methylammonium lead iodide based perovskites: cytotoxicity studies. Toxicol Res 2016;5:407–19.
[16] Liang C, Wu Z, Li P, Fan J, Zhang Y, Shao G. Chemical bath deposited rutile TiO_2 compact layer toward efficient planar heterojunction perovskite solar cells. App Surf Sci 2017;391:337–44.
[17] Snaith HJ. Perovskites: the emergence of a new era for low-cost, high-efficiency solar cells. J Phys Chem Lett 2013;4:3623–30.
[18] Stranks SD, Eperon GE, Grancini G, Menelaou C, Alcocer MJP, Leijtens T, et al. Electron-hole diffusion lengths exceeding 1 micrometer in an organometal trihalide perovskite absorber. Science 2013;342:341–4.
[19] Wu N, Shi C, Ying C, Zhang J, Wang M. PbICl: A new precursor solution for efficient planar perovskite solar cell by vapor-assisted solution process. App Surf Sci 2015;357:2372–7.
[20] Xing G, Mathews N, Sun S, Lim SS, Lam YM, Grätzel M, et al. Long-range balanced electron- and hole-transport lengths in organic-inorganic $CH_3NH_3PbI_3$. Science 2013;342:344–7.
[21] Yan J, Ke X, Chen Y, Zhang A, Zhang B. Effect of modulating the molar ratio of organic to inorganic content on morphology, optical absorption and photoluminescence of perovskite $CH_3NH_3PbBr_3$ films. App Surf Sci 2015;351:1191–6.
[22] Zhao Y, Zhu K. Efficient planar perovskite solar cells based on 1.8 eV band gap $CH_3NH_3PbI_2Br$ nanosheets via thermal decomposition. J Am Chem Soc 2014;136:12241–4.
[23] Zhou H, Chen Q, Li G, Luo S, T-b Song, Duan H-S, et al. Interface engineering of highly efficient perovskite solar cells. Science 2014;345:542–6.
[24] Hao F, Stoumpos CC, Cao DH, Chang RPH, Kanatzidis MG. Lead-free solid-state organic-inorganic halide perovskite solar cells. Nat Photonics 2014;8:489–94.
[25] Liao W, Zhao D, Yu Y, Grice CR, Wang C, Cimaroli AJ, et al. Lead-free inverted planar formamidinium tin triiodide perovskite solar cells achieving power conversion efficiencies up to 6.22%. Adv Mater 2016;28:9333–40.
[26] Noel NK, Stranks SD, Abate A, Wehrenfennig C, Guarnera S, Haghighirad A-A, et al. Lead-free organic-inorganic tin halide perovskites for photovoltaic applications. Energy Environ Sci 2014;7:3061–8.
[27] Anaya M, Correa-Baena JP, Lozano G, Saliba M, Anguita P, Roose B, et al. Optical analysis of $CH_3NH_3Sn_xPb_{1-x}I_3$ absorbers: a roadmap for perovskite-on-perovskite tandem solar cells. J Mater Chem A 2016;4:11214–21.
[28] Ogomi Y, Morita A, Tsukamoto S, Saitho T, Fujikawa N, Shen Q, et al. $CH_3NH_3Sn_xPb_{(1-x)}I_3$ perovskite solar cells covering up to 1060 nm. J Phys Chem Lett 2014;5:1004–11.
[29] Zuo F, Williams ST, Liang P-W, Chueh C-C, Liao C-Y, Jen AK-Y. Binary-metal perovskites toward high-performance planar-heterojunction hybrid solar cells. Adv Mater 2014;26:6454–60.
[30] Wang JT-W, Wang Z, Pathak S, Zhang W, deQuilettes DW, Wisnivesky-Rocca-Rivarola F, et al. Efficient perovskite solar cells by metal ion doping. Energy Environ Sci 2016;9:2892–901.
[31] Wang Z-K, Li M, Yang Y-G, Hu Y, Ma H, Gao X-Y, et al. High efficiency Pb–In binary metal perovskite solar cells. Adv Mater 2016;28:6695–703.
[32] Pérez-del-Rey D, Forgács D, Hutter EM, Savenije TJ, Nordlund D, Schulz P, et al. Strontium insertion in methylammonium lead iodide: long charge carrier lifetime and high fill-factor solar cells. Adv Mater 2016;28:9839–45.
[33] Navas J, Sanchez-Coronilla A, Gallardo JJ, Cruz Hernandez N, Pinero JC, Alcantara R, et al. New insights into organic–inorganic hybrid perovskite $CH_3NH_3PbI_3$ nanoparticles. An experimental and theoretical study of doping in Pb2+ sites with Sn2+, Sr2+, Cd2+ and Ca2+.. Nanoscale 2015;7:6216–29.
[34] Wu M-C, Chan S-H, Jao M-H, Su W-F. Enhanced short-circuit current density of perovskite solar cells using Zn-doped TiO_2 as electron transport layer. Sol Energy Mater Sol Cells 2016;157:447–53.
[35] Gate LF. Comparison of the photon diffusion model and kubelka-munk equation with the exact solution of the radiative transport equation. Appl Optics 1974;13:236–8.
[36] Pazoki M, Jacobsson TJ, Hagfeldt A, Boschloo G, Edvinsson T. Effect of metal cation replacement on the electronic structure of metalorganic halide perovskites: replacement of lead with alkaline-earth metals. Phys. Rev. B 2016;93:144105.
[37] Bozack M J, Bryant K W. Elemental Lead by XPS. Surf. Sci. Spectra 1998;1:324–7.
[38] Morgan W E, Van Wazer JR. Binding energy shifts in the x-ray photoelectron spectra of a series of related Group IVa compounds. J. Phys. Chem 1973;77:964–9.
[39] Powell CJ. Recommended Auger parameters for 42 elemental solids. J. Electron Spectrosc Relat 2012;185:1–3.